Water Practice & Technology

IWA PUBLISHING

Water Practice & Technology Vol 17 No 1, 175 doi: 10.2166/wpt.2021.127

Process simulation of modelled reverse osmosis for desalination of seawater

Nurudeen Salahudeen

Department of Chemical and Petroleum Engineering, Bayero University, Kano, Nigeria
E-mail: nusdeen@yahoo.co.uk

NS, 0000-0002-7537-8011

ABSTRACT

Model equations for prediction of process parameters of reverse osmosis for desalination of seawater were developed via mathematical derivation from basic equations for the reverse osmosis process. A model equation relating the interfacial solute concentration (C_{si}) with the process pressure difference (ΔP) was developed. Taking the ΔP of reverse osmosis as the basic independent variable, further model equations relating other process parameters such as the solute concentration polarity (Γ), water flux (J_w), osmotic pressure ($\Delta\pi$), water output rate (q), power density (Pd) and specific energy consumption (SEC) were developed. Simulation of hypothetical reverse osmosis data using Microsoft Excel Worksheet and Microsoft Windows 10 on a 64-bit operating system was carried out. Simulation results showed that the optimum fluid bulk concentration was $C_o = 0.0004$ mole/cm^3. The optimum rate of increase in the solute rejection factor per unit rise in ΔP was 0.45%. The optimum solute rejection factor was 97.6%. The optimum water output rate, specific energy consumption and power density were 103.2 L/h, 3.65 kWh/m^3 and 6.09 W/m^2, respectively.

Key words: desalination of seawater, modeling, process parameters, reverse osmosis, simulation

HIGHLIGHTS

- Mathematical model for simulation of reverse osmosis (RO) process was developed.
- The RO process operated favourably at $C_o \leq 0.0004$ mole/cm^3.
- The simulated RO process operated optimally at ΔP of 3.7 atm.
- The optimum water output rate was 103.2 L/h.
- The optimum solute rejection factor was 97.6%.
- The optimum specific energy consumption was 3.65 kWh/m^3.

GRAPHICAL ABSTRACT

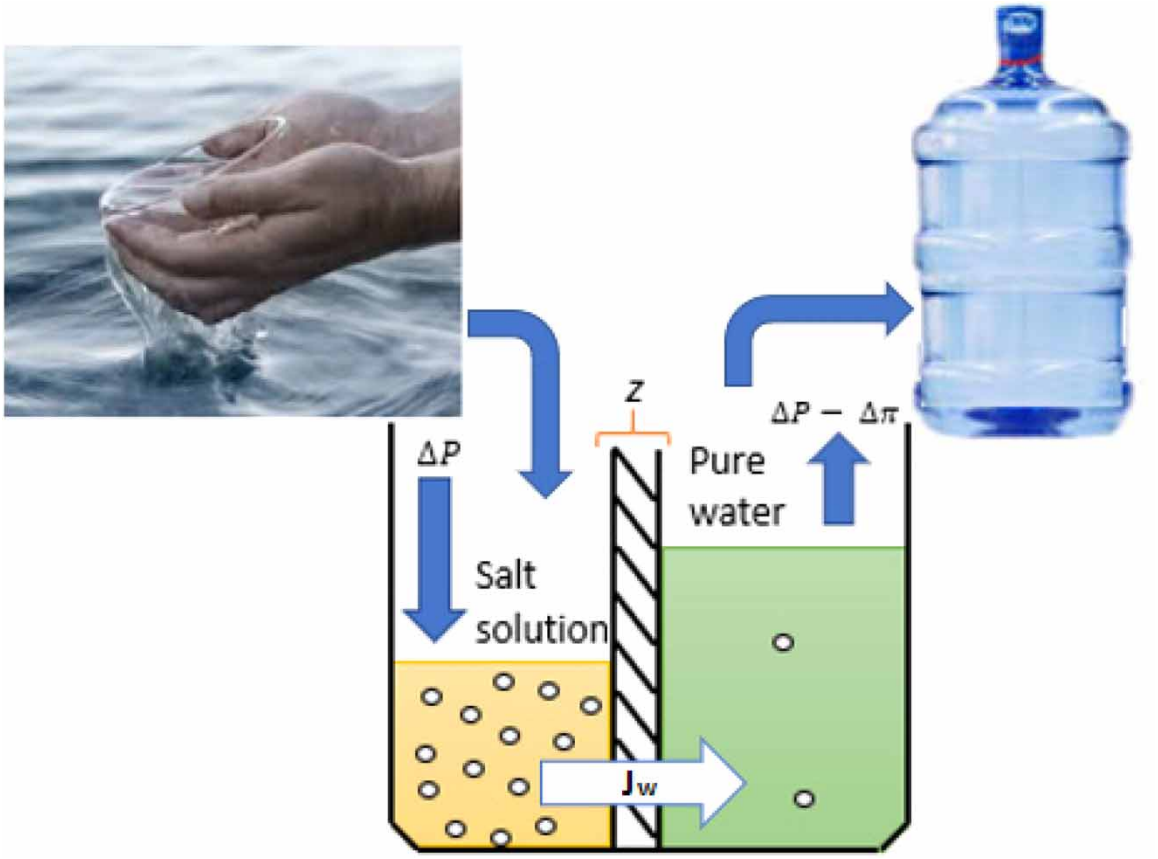

1. INTRODUCTION

Fresh water available for human consumption is continuously threatened by an exponentially increasing depletion resulting from the combined factors of environmental pollution and global warming. This critical challenge has made it crucial for man to seek an alternative means of sourcing the all-time indispensably needed fresh water for human and animal consumption and other day-to-day needs of man. Desalination of seawater via reverse osmosis process has become a prominent method of sourcing fresh water for human consumption since the 1960s (Loeb & Sourirajan 1963). Reverse osmosis became a practical process with the discovery of asymmetric cellulose-acetate membranes by Loeb and Sourirajan in 1962 (Loeb & Sourirajan 1963). Before the discovery of reverse osmosis, thermal operation involving evaporation and condensation processes had been the method for desalination of seawater. Today, reverse osmosis accounts for at least 64% of industrial desalination of seawater while the thermal process accounts for just about 34% (Henthorne 2009). Other low-scale industrial processes for desalination of seawater include nanofiltration, membrane distillation and electrodialysis (Khawaji *et al.* 2008). The major drawback of the thermal method is its high energy consumption, which lowers the economy of the process for commercial water desalination.

Reverse osmosis is a membrane separation method whereby miscible solutions of different concentration are separated by a membrane that is permeable to the solvent but nearly impermeable to the solute (Kim *et al.* 2020; Ligaraya *et al.* 2020; Monjezi *et al.* 2020). Reverse osmosis derives its name from the technical meaning of the process. It is an opposite operation of the osmosis process. In the osmosis process, the driving force of the process is the solvent activity. The solvent diffuses in the direction of increasing solvent activity. Therefore, the solvent diffuses from the less concentrated solution region where the solvent activity is higher to the more concentrated solution region, where the solvent activity is lower (McCabe *et al.* 1993). The flow of solvent from the less concentrated region to the more concentrated region is driven by the osmotic pressure ($\Delta\pi$). Figure 1 shows a pictorial illustration of the reverse osmosis process.

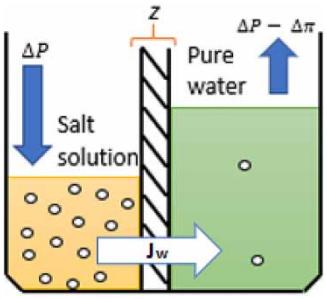

Figure 1 | Pictorial illustration of reverse osmosis process.

In order to achieve reverse osmosis, the pressure of the concentrated solution must be raised to counter the osmotic pressure. As the pressure of the concentrated solution is raised, the osmotic diffusion is slowed down until the activity gradient across the two ends of the membrane is lowered. At the point where the activity gradient is zero, the osmotic diffusion is stopped. A further increase in the pressure of the concentrated solution will result in diffusion of solvent from the concentrated region to the dilute region (McCabe *et al.* 1993; Cornelissen *et al.* 2021). If pure solvent is on one side of the membrane, the pressure required in the concentrated region to achieve zero solvent activity gradient is called the osmotic pressure of the solution, denoted by ($\Delta\pi$). To achieve the reverse osmosis process, the pressure applied on the concentrated region must be greater than $\Delta\pi$.

Membranes used in reverse osmosis are mostly flexible films of synthetic polymers prepared to have a high permeability for water molecules only. Reverse osmosis membranes are effectively non-porous and, therefore, exclude particles and even many low molar mass species such as salt ions, organics and other impurities in water (Loeb & Sourirajan 1963; Amjad 1993; McCabe *et al.* 1993). Only water molecules gain access across the membrane. Chemically they are typically made of either cellulose acetate or polysulfone coated with aromatic polyamides. These materials are suitable for use as reverse osmosis membranes because they have a high permeability for water and low permeabilities for dissolved salts. Reverse osmosis membranes are applied either as layers of films or as hollow fibres depending on the design of the desalination process (Amjad 1993; McCabe *et al.* 1993). However, for industrial applications the hollow fibres are applied.

It has been reported that 100% rejection of solute is not possible in practice for one stage reverse osmosis (McCabe *et al.* 1993). One stage operation can only achieve percentage solute rejection of 97–99%. To achieve approximately 100% rejection of solute, multiple stage reverse osmosis plants are usually employed in industrial desalination of seawater (Cath *et al.* 2006; Kim *et al.* 2020). Figure 2 shows a typical two-stage, three-pass reverse osmosis for desalination of seawater. Each stage consists of three filters; two parallel filters in series operation with the third filter. In the first stage operation, the feed seawater is introduced through the shell of the reverse osmotic filters and the permeate is collected via the lumen of the membrane tube. The permeate collected from the first stage is introduced as feed into the second stage and the permeate from the second stage is collected as the purified water.

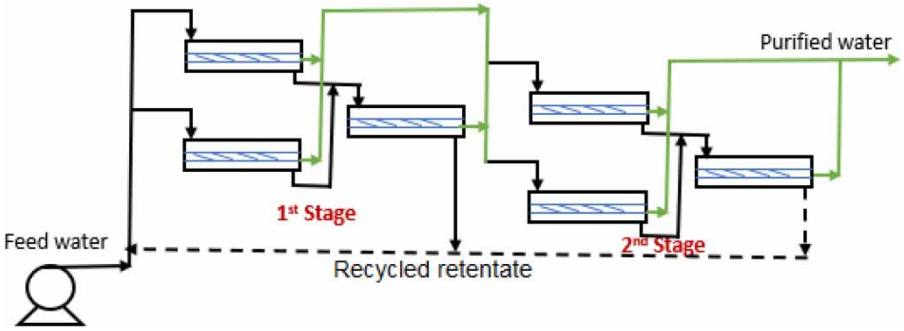

Figure 2 | Flow diagram for a two-stage reverse osmosis process.

2. MATERIALS AND METHODS

Mathematical modelling of the solute interfacial concentration of reverse osmosis process in relation to the process ΔP was carried out from the basic equations for the reverse osmosis process adopting the Hagen-Poiseuille

model (McCabe *et al.* 1993) of the flow model. Further model equations relating the ΔP with solute concentration polarity (Γ), water flux (J_w) and osmotic pressure ($\Delta\pi$) were modelled. Using the model developed, simulation of a typical reverse osmosis process model was run on Intel(R) Celeron(R) 2955 U @ 1.45 GHz via Microsoft Excel Worksheet. Process conditions used for this study were adapted by McCabe *et al.* (1993). The temperature used was 25 °C and variable ΔP of 1–9 atm. A lumen permeator made of asymmetric cellulose acetate membranes having thickness of 200 μm and variable membrane filter length was adopted for the simulation (Scott 1998; Paul 2004). Given that the viscosity of water at 25 °C was 0.000891 kg/m-s, mass transfer coefficient based on concentration across the membrane was 5.841×10^{-5} m/s and the constant due to gravity was 9.81 m/s^2.

2.1. Modeling theory

In the reverse osmosis process, separation normally depends on differences in diffusivity; the retentate and permeate phases are separated by the membrane, and differences in the equilibrium solute distribution as well as differences in diffusivity determine the purity of the extract**.** Permeation of liquids occurs by a solution-diffusion mechanism. The selectivity depends on the solubility ratio as well as the diffusivity ratio. The permeate is nearly pure water at about 1 atm and having activity slightly less than 1.0. Very high pressure is normally applied to the feed solution to make the activity of the water slightly greater than that in the permeate. This will provide an activity gradient across the membrane and the concentration of water in the product will be higher than that in the feed (McCabe *et al.* 1993).

Considering a typical reverse osmosis shown in Figure 1, the water flux (J_W) through the membrane in L/m^2-h or multiplied by conversion factor of 2.78×10^{-7} for a value in m/s is given by Equation (1) (McCabe *et al.* 1993).

$$J_W = \frac{C_w D_w v_w}{RT}\left(\frac{\Delta P - \Delta\pi}{z}\right) \tag{1}$$

where

C_w = average water concentration in g/cm^3
D_w = diffusivity of water through the membrane in cm^2/s
v_w = partial molar volume of water in cm^3/g
ΔP = process pressure difference across both ends of the membrane in atm
$\Delta\pi$ = osmotic pressures across the feed and product in atm
z = cross sectional thickness of the membrane in μm
R = gas constant, equals 8.314 J/mol-K
T = absolute temperature of the process measured in Kelvin.

Equation (1) is a key basic model equation for reverse osmosis operations (Salahudeen 2020). In industrial operation, each of the stages of reverse osmosis is made of a bundle of hollow-fibre membranes having thousands of closely packed fibres sealed in a metal cylinder. The filtration process is operated in a shell and tube configuration. The feed solution is introduced radially across the fibres from the shell side and product water collected from the fibre lumens at the tube side. For a typical reverse osmosis process for desalination of water having known viscosity (μ), through a known length of fibre tube (L), having tube diameter (d) and the average velocity of flow ($\bar{v}$) inside the tube. The flow through the membrane fibre is laminar (McCabe *et al.* 1993). The pressure gradient caused by friction due to the membrane surface is given by the derivative form of the Hagen-Poiseuille equation given as Equation (2).

$$\frac{dP}{dL} = \frac{32\mu\bar{v}}{gd^2} \tag{2}$$

where g is a constant due to gravity, having a value of 9.81 m/s^2

The incremental change in the volumetric flow rate is equivalent to the flux per unit wall area multiplied by the incremental area, expressed as Equation (3).

$$\pi\frac{d^2}{4}d\bar{v} = J_w \pi d\,\mathrm{dL} \tag{3}$$

Therefore, we have:

$$\frac{d\bar{v}}{dL} = \frac{4\,J_w}{d} \tag{4}$$

The increase in osmotic pressure due to increase in salt concentration along the length of the tube is counterbalanced by the pressure build-up inside the fibres. Therefore, assuming J_w is constant, integration of Equation (4) gives:

$$\int d\bar{v} = \int \frac{4\,J_w}{d}\,dL \tag{5}$$

$$\bar{v} = \frac{4\,J_w}{d}\,\mathrm{L} \tag{6}$$

Therefore, substituting Equation (6) into (2) we have:

$$\frac{dP}{dL} = \frac{32\mu}{gd^2} \times \frac{4\,J_w}{d}\,\mathrm{L} \tag{7}$$

$$dP = \frac{128\mu L J_w}{gd^3}\,\mathrm{dL} \tag{8}$$

Integrating both sides of Equation (8) taking the limits of P_o to P, for the pressure and 0 to L, for the tube length, we have:

$$\int_{P_o}^{P} dP = \frac{128\mu J_w}{gd^3} \int_0^L L\,dL \tag{9}$$

$$\mathrm{P} - \mathrm{P}_o = \frac{128\mu J_w}{gd^3} \times \frac{L^2}{2} \tag{10}$$

Hence,

$$\Delta P = \frac{64\mu J_w L^2}{gd^3} \tag{11}$$

Concentration polarization is a major factor that determines the efficiency of a reverse osmosis process. Concentration polarization is the concentration variation resulting from nearly complete rejection of solute by the membrane, thereby resulting into to a higher solute concentration at the membrane interface compared to the bulk solute concentration in the solution (Lilanea *et al.* 2020).

The polarization factor is defined by Equation (12) (McCabe *et al.* 1993):

$$\Gamma = \frac{C_{si} - C_s}{C_s} = \frac{J_w f}{k_c} \tag{12}$$

where f is the solute rejection factor of the membrane; $f = \left(1 - \frac{C_o}{C_s}\right) \times 100\%$

C_o = bulk concentration of permeate in mole/cm^3

C_s = solute concentration in mole/cm^3

k_c = mass-transfer coefficient for diffusion of the solute away from the membrane in m/s

For a steady process, C_s and C_w are predetermined constants. Hence, f is constant.

From Equation (12), we have:

$$J_w = \frac{(C_{si} - C_s)k_c}{fC_s} \tag{13}$$

Substituting (13) into (11) we have:

$$\Delta P = \frac{64\mu L^2 k_c}{fgd^3} \times \frac{(C_{si} - C_s)}{C_s} \tag{14}$$

$$\Delta P = \frac{64\mu L^2 k_c}{fgd^3} \times \frac{\Delta C_s}{C_s} \tag{15}$$

Taking the total incremental change for the solute pressure and the solute concentrations, we have:

$$dP = \frac{64\mu L^2 k_c}{fgd^3} \times \frac{\mathrm{d}C_s}{C_s} \tag{16}$$

For a steady state process, the bulk solute concentration ($C_o = C_s$) can be assumed to be constant throughout the operation. Integrating both sides of Equation (16) taking the limits of P_o to P for the pressure and C_o to C_{si} for the solute concentration, we have:

$$\int_{P_o}^{P} dP = \frac{64\mu L^2 k_c}{fgd^3} \int_{C_o}^{C_{si}} \frac{\mathrm{d}C_s}{C_s} \tag{17}$$

$$\mathrm{P} - P_o = \frac{64\mu L^2 k_c}{fgd^3} \mathrm{In}\,[C_{si} - C_o) \tag{18}$$

Hence,

$$\Delta P = \frac{64\mu L^2 k_c}{fgd^3} \mathrm{In}[C_{si} - C_o) \tag{19}$$

Therefore, given an osmotic process operating at a known bulk solute concentration C_o in g/cm^3 or mole/cm^3, the C_{si} at the membrane surface can be determined at any given ΔP. Equation (20) is the central operation model relating ΔP with the C_{si}.

$$C_{si} = C_o e^{\left(\frac{\Delta P(fgd^3)}{64\mu L^2 k_c}\right)} \tag{20}$$

$$C_{si} = C_o e^{Q\Delta P} \tag{21}$$

where

$$\mathrm{Q} = \frac{fgd^3}{64\mu L^2 k_c} \text{ and } C_o = C_s \tag{22}$$

Q is called the lumpsum reverse osmosis constant parameter.

Model equations relating the ΔP to polarity and water flux could be developed by substituting Equations (21) into Equations (12) and (13), respectively.

$$\Gamma = (e^{Q\Delta P} - 1) \tag{23}$$

$$J_w = \frac{C_s k_c}{fC_s}(e^{Q\Delta P} - 1) \tag{24}$$

The model equation relating the process ΔP and the osmotic pressure ($\Delta\pi$) was also developed as Equation (25).

$$\Delta\pi = \mathrm{RT}\Delta C_s = \mathrm{RT}C_s(e^{Q\Delta P} - 1) \tag{25}$$

The power density of the RO in W/m^2 is given by Equation (26) and the specific energy consumption (SEC) in kWh/m^3 is given by Equation (27).

$$\mathrm{P} = \Delta \mathrm{P}\, J_w \tag{26}$$

$$\mathrm{SEC} = \frac{3.6 \Delta \mathrm{P}\, J_w}{L} \tag{27}$$

Assuming the aspect ratio (L/D) of the membrane lumen is 4. Then the cross-sectional area of the filtration lumen is given as Equation (28):

$$\mathrm{A} = \frac{\pi L^2}{64} \tag{28}$$

Therefore, if J_w is measured in L/m^2-h and L in meter, the treated water output rate in L/h is given as Equation (29).

$$q = J_w \frac{\pi L^2}{64} \tag{29}$$

3. SIMULATION RESULTS AND DISCUSSION

Considering a hypothetical reverse osmosis operation for seawater with membrane filter length of 2 m and process conditions as given in Section 2, process simulation of the RO for desalination of seawater was carried out for a variable bulk solute concentration of the feed seawater ranged between 0.0001 and 0.001 mole/cm^3. Evaluation of the lumpsum reverse osmosis constant parameter (Q) in Equation (22) gave a value of 5.867×10^{-6} m^2/g for a constant solute rejection factor of 99.6%.

3.1. Determination of the optimum bulk solute concentration for the RO operation

Considering variable values of the feed bulk solute concentration (C_o), simulation results of the process C_{si} against water flux at variable C_o are presented in Figure 3(a) and 3(b). It could be observed that the response of the C_{si} to the water flux was C_o dependent. The C_{si} response was not only C_o dependent but also region sensitive. The two clear regions of the bulk solute concentration sensitivity were (i) $C_o \leq 0.0004$ mole/cm^3 presented in Figure 3(a) and (ii) $C_o > 0.0004$ mole/cm^3 presented in Figure 3(b). Within the first region, C_{si} generally showed a consistent trend of linear and gradual increase as the water flux increased. The trend was similar throughout this region. The average value of C_{si} in this region was 0.000–0.066 mole/cm^3, corresponding to a water flux value range of 0–40,000 L/m^2-h. At lower values of C_{si} less than 0.01 mole/cm^3, all the graphs converged and had about the same low water flux values. The narrow region covered by $C_o \leq 0.0004$ mole/cm^3 accounted for 77 iteration points of the process. Within the second region, both water flux and C_{si} values approached infinity at all $C_o$values. Actual value of C_{si} in the second region was 1×10^6–12×10^6 mole/cm^3, corresponding to a water flux value range of 1×10^6–3×10^{12} L/m^2-h for just 20 iteration points of the process. This showed that the process operation region ≤ 0.0004 mole/cm^3 was the region that favourably described the RO process as it closely described the real RO conditions. The region >0.0004 mole/cm^3 was outrageously in variance with real RO process conditions as the process solute interfacial concentration and water flux were tending to infinity. The low range C_{si} values observed at $C_o \leq 0.0004$ mole/cm^3 was due to unhindered forward flow of the water, whereas at $C_o > 0.0004$ mole/cm^3 outrageously high values of C_{si} implied concentration build-up on the bulk side of the membrane. Concentration build-up has been reported to result in diffusive flow-back, which will retard the progress of the RO process (Mulder 1997; Koseoglu *et al.* 2018).

Figure 4(a) and 4(b) further show the trend of sensitivity of the interfacial solute concentration with slight increase in ΔP. (A) shows the effect of a 20 and 40% step increase in ΔP from 1.0 atm to 1.2 and 1.4 atm, while (B) shows the effect of another 40, 60 and 80% step increase in ΔP from 1.0 atm to 1.4, 1.6 and 1.8 atm. Considering the step increase (A), it could be observed that the first region ($C_o \leq 0.0004$ mole/cm^3) was a favourable operation region showing no sensitivity to the slight increase in the process ΔP as the interfacial solute concentration remained the same for each solute bulk concentration. It could be observed that within

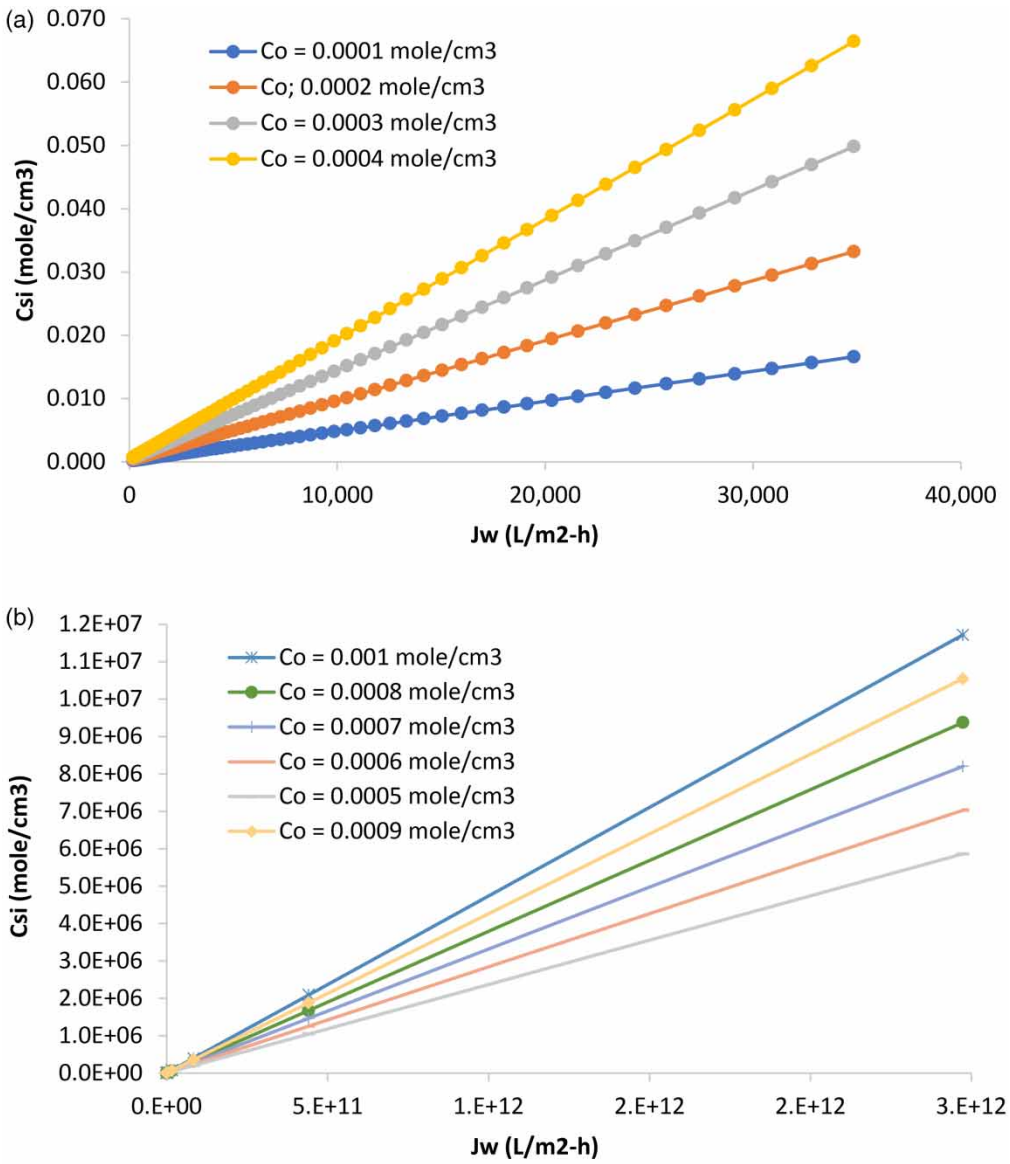

Figure 3 | Interfacial solute concentration against water flux at (a) $C_o \leq 0.0004$ mole/cm^3 (b) $C_o > 0.0004$ mole/cm^3.

the second region the response of $C_{si}$was quite significant. At bulk solute concentration of 0.0005 mole/cm^3, the increase in C_{si} values for 20 and 40% increase in ΔP were 300% and 1700%, respectively. At bulk solute concentration of 0.0006 mole/cm^3, similar high sensitivity of C_{si} for slight change in ΔP was observed. The increase in C_{si} values for 20 and 40% increase in the process pressure were 300% and 2000%, respectively. This pattern was maintained until bulk solute concentration of 0.001 where the increase in C_{si} values for 20 and 40% increase in ΔP were 250% and 1,650%, respectively. The average value of C_{si} within the bulk solute concentration region of $0.0005 \leq C_o \leq 0.001$ mole/cm^3 was constant at process ΔP increase of 20 and 40%.

Figure 4(b) shows similar response of C_{si} over the two regions of the bulk solute concentration. Similarly, it could be observed that the first region ($C_o \leq 0.0004$ mole/cm^3) was a good operation region showing no sensitivity to increase in ΔP. The C_{si} remained the same for each solute bulk concentration as observed in Figure 4(a). The response of C_{si} was outrageously high in the second region ($C_o > 0.0004$ mole/cm^3). At bulk solute concentration of 0.0005 mole/cm^3, the increase in C_{si} values for 60 and 80% increase in ΔP were 11,000% and 89,400%, respectively. This pattern was maintained until bulk solute concentration of 0.001 mole/cm^3 where the increase in C_{si} values for 60 and 80% increase in the process pressure were 11,100% and 89,450%, respectively. Therefore, it could be observed that the response of C_{si} to slight increase in ΔP became more outrageous and was tending to infinity as the step increment advanced. The very high C_{si}

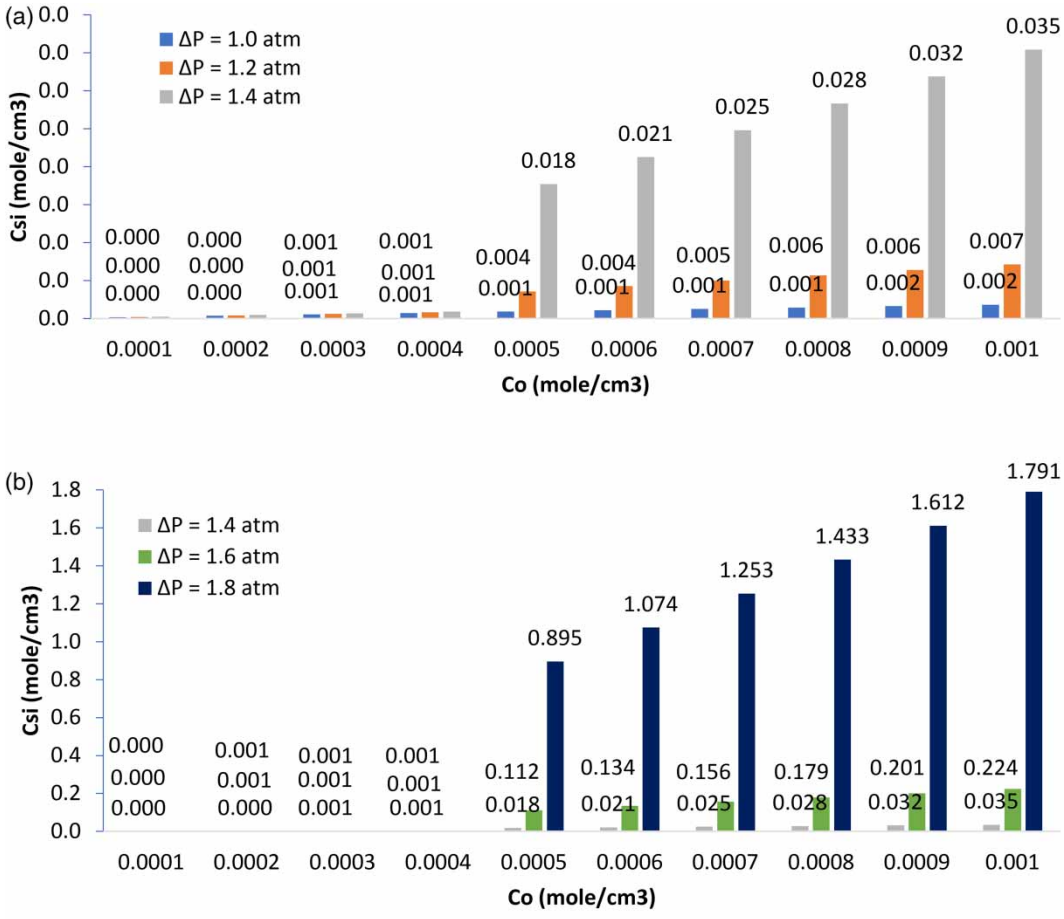

Figure 4 | Interfacial solute concentration profile against bulk solute concertation at variable ΔP (a) 20 and 40% increase in ΔP from 1.0 atm (b) 40, 60 and 80% increase in ΔP from 1.0 atm.

experienced at C_o >0.0004 mole/cm^3 was expected to retard the RO process due to diffusive flow-back (Koseoglu *et al.* 2018). This suggested that the second region was not a favourable operational region for the RO. Hence, the optimum point of the RO operation was at C_o value of 0.0004 mole/cm^3 being the highest point of least process response in C_{si} in the region favourable for the RO operations.

3.2. Impact of solute interfacial concentration on ΔP at variable solute concentration of RO

Figure 5(a) and 5(b) show trends of ΔP against C_{si} for a seawater feed having variable bulk solute concentrations. Figure 5(a) shows the simulation for the RO process having $C_o \leq 0.0004$ mole/cm^3; it could be observed that the solute interfacial concentration at each value of the C_o followed the same pattern of continuous non-linear increase with rise in the ΔP. At low pressure range lower than 3 atm, the C_{si} behaviour at each C_o value was close to zero and almost the same for all the simulated conditions. However, at higher ΔP above 3 atm, the simulated process diverged attaining higher values and a clear difference could be observed in the respective response of the process C_{si} against ΔP for each C_o. At particular constant ΔP, the C_{si} value became higher as the bulk solute concentration increased from 0.0001 mole/cm^3 to 0.0004 mole/cm^3. Implying that at C_o of 0.0004 mole/cm^3 the RO process was at optimum in terms of separation of the seawater. The observed trend of continuous increase of C_{si} with increasing ΔP was similar to the trend reported by Idrees (2020) and Cath *et al.* (2006). Figure 5(b) shows the simulation for the RO process having C_o >0.0004 mole/cm^3. It could be observed that the C_{si} at each value of C_o ranging from 0.0005–0.001 mole/cm^3 showed the same pattern having two-part curve. The first part of the curve was basically horizontal where the C_{si} was constantly zero at all ΔP value from 0–3.7 atm. The second part of the curve was basically vertical where C_{si} values were tending to infinity at all ΔP higher than 3.7 atm. This clearly showed the divergent point earlier noticed in the process simulation behaviour at $C_o \leq$ 0.0004 mole/cm^3, the divergence in the process behaviour occurred at ΔP of 3.7 atm. This process behaviour

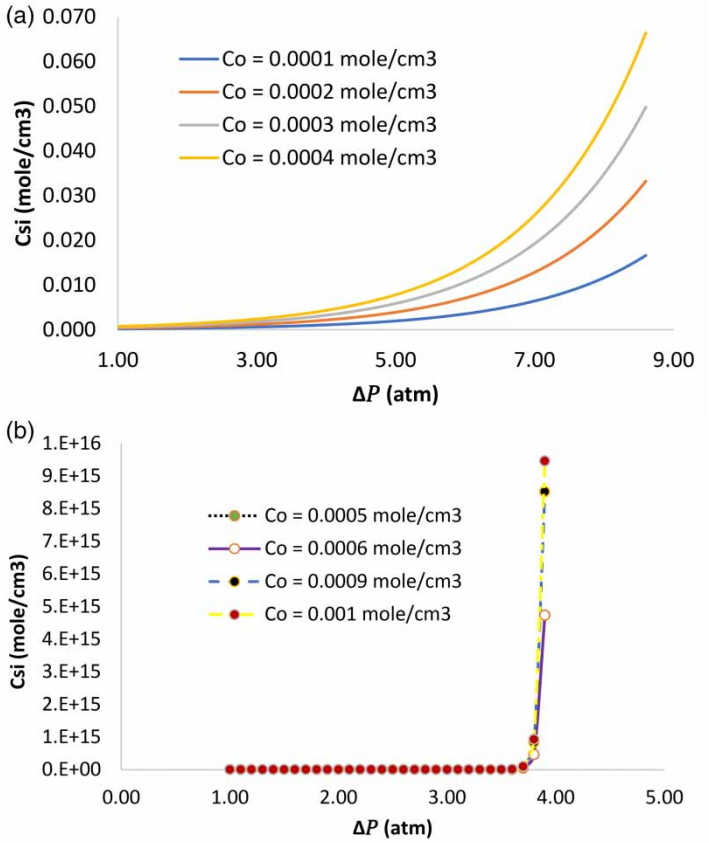

Figure 5 | Interfacial solute concentration profile against ΔP at (a) $C_o \leq 0.0004$ mole/cm^3 (b) $C_o > 0.0004$ mole/cm^3.

observed in Figure 5(b) further suggested that the RO process was not suitable at a$C_o > 0.0004$ mole/cm^3. Hence it follows that C_{si} showed gradual trend of increase with increasing ΔP for $C_o \leq 0.0004$ mole/cm^3 due to absence of concentration build-up on the bulk side of the membrane, whereas at $C_o > 0.0004$ mole/cm^3 concentration build-up resulted into diffusive flow-back (Mulder 1997; Koseoglu *et al.* 2018). The point of onset of diffusive flow-back was at $\Delta P > 3.7$ atm.

Figure 6 shows variation of the average fluid flow velocity and water flux against the process ΔP at optimum C_o of 0.0004 mole/cm^3. It could be observed that both the responses of water flux and average fluid velocity against ΔP showed the same pattern of linear increase with increasing ΔP. The pattern observed in both cases were

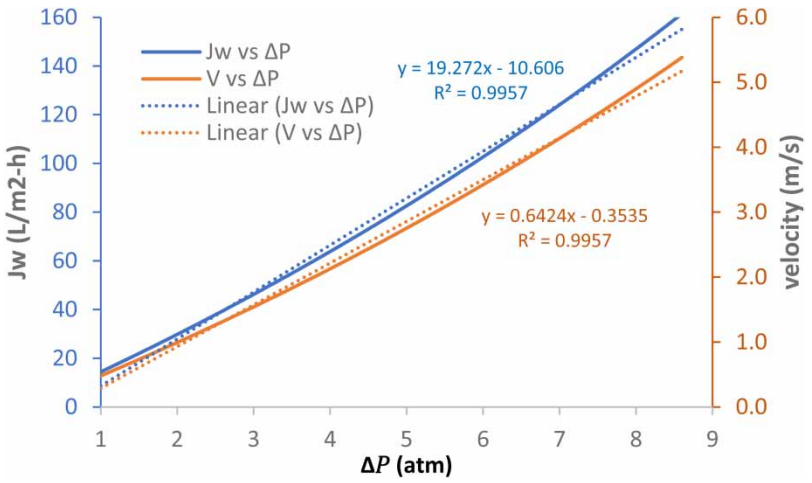

Figure 6 | Water flux and process velocity against process ΔP.

similar to the pattern observed for the process C_{si} against ΔP and J_w at $C_o \leq 0.0004$ mole/cm^3. Using the Lee *et al.* (1981) osmosis direction characterization, the water flux against ΔP graph confirmed that the process proceeded in the reverse osmosis direction.

Figure 7 shows the solute rejection profile against ΔP at the optimum C_o of 0.0004 mole/cm^3. The least solute rejection of 44.8% was observed at the least ΔP of 1.0 atm. Three distinct profile behaviours could be analysed, these are region #1; region #2; and region #3. Region #1 featured a continuous linear rise in solute rejection with increasing ΔP until around solute rejection factor of 83% corresponding to ΔP of 3.0 atm. Within this region, the average rate of increase in the solute rejection factor per unit rise in ΔP was 2 unit. Region #2 which stretches from 3.0–6.0 atm corresponded to solute rejection factor of 83% – 97.6%, respectively. This Region showed a relatively lower rate of increase in solute rejection factor; the average rate of increase in solute rejection factor per unit rise in ΔP in this region was 0.5 unit. Further analysis of the profile at region #3 showed the least response of solute rejection factor against increase in ΔP. Region #3 stretches from ΔP values of 6.0–8.6 atm corresponding to solute rejection factor values of 97.6% – 99.4%, respectively. The average rate of increase in solute rejection factor per unit rise in ΔP in this least region was 0.09 unit. An overview analysis of the solute rejection against ΔP of the reverse osmosis process showed a logarithmic continuous increase in the solute rejection for a continuous increase in ΔP. Similar trend has been reported by Jang *et al.* (2018). Although region #3 could be considered as the region of highest solute rejection condition having the maximum solute rejection factor, however, the rate of increase in the solute rejection factor per unit rise in ΔP in this region was the least. Therefore, region #2 could be considered as the region of optimum solute rejection response as it was the intermediate region having a balance of moderate solute rejection value up to 97.6% and a moderate rate of increase in the solute rejection factor per unit rise in ΔP. Region #2 was also considered the optimum region because at high solute rejection of 97.6%, salt passage in the direction of the water flow would be negligible (McCutcheon & Elimelech 2006). Although the maximum solute rejection factor at region #2 was 2.4% lower than the maximum value at region #3 but the average rate of increase in the solute rejection factor per unit rise in ΔP at region #2 was 5.6 times higher than the rate at region #3.

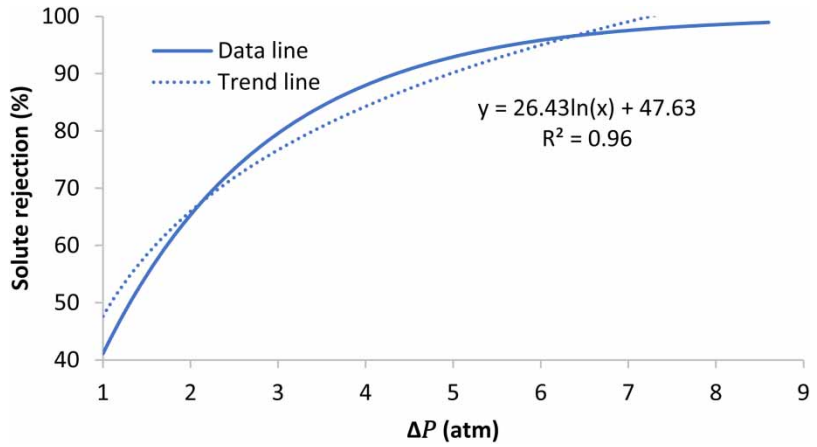

Figure 7 | Solute rejection profile against process ΔP.

3.3. Impact of interfacial solute concentration on process parameters

Figure 8 shows water flux and solute concentration polarity against C_{si} at the optimum C_o of 0.0004 mole/cm^3. It could be observed that both the water flux and solute concentration polarity increased linearly with C_{si}. The trend observed agreed with what was reported by Jang *et al.* (2018). Similar trend of almost equal rate of increase was observed in the water flux and the solute concentration polarity for the entire C_{si} values range of 0.00045–0.0007 mole/cm^3. The two graphs intersected at C_{si} value of 0.000575 mole/cm^3 making each of the graphs form a mirror image of the other. A slight variation was observed in the rates of increase of water flux and polarity at either side of the intersection point. The point of intersection corresponded to J_w value of 86 L/m^2-h, applying

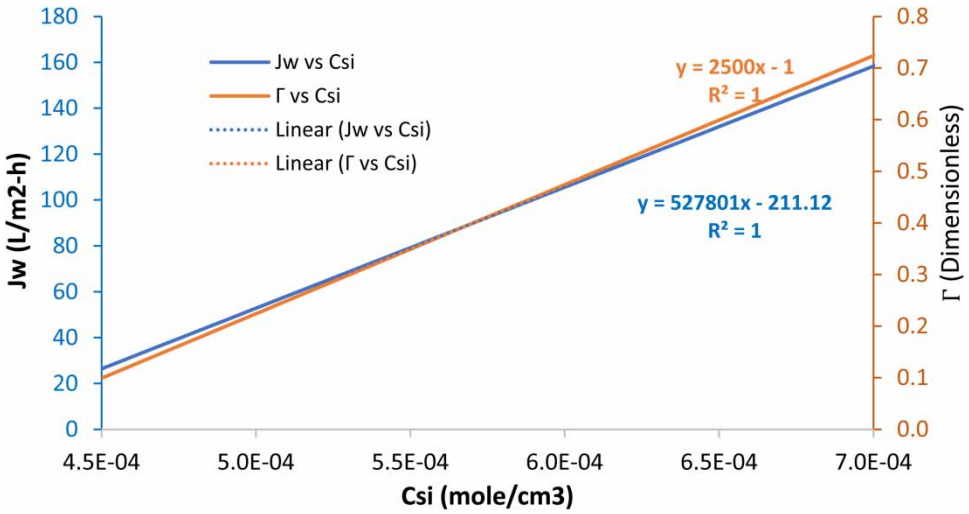

Figure 8 | Water flux and concentration polarity profiles against C_{si}.

Equation (30), the relationship between J_w and ΔP obtained from Figure 6, we have:

$$\Delta P = \frac{J_w + 10.606}{19.272} \tag{30}$$

This point corresponded to ΔP value of 5.0 atm. Therefore, the rate of increase of polarity was slightly lower than the rate of increase of water flux at C_{si} <0.000575 mole/cm^3 corresponding to ΔP <5.0 atm while the rate of increase of polarity was slightly higher than the rate of increase of water flux at C_{si} >0.000575 mole/cm^3 corresponding to ΔP >5.0 atm. This further suggested that the favourable operation region was the region covered by C_{si} <0.000575 mole/cm^3 and ΔP <5.0 atm.

Figure 9 shows the variation in solute rejection factor against C_{si} at the optimum C_o of 0.0004 mole/cm^3. It could be observed that the minimum solute rejection of 41% was recorded against C_{si} of 0.00068 mole/cm^3. The value of solute rejection factor raised exponentially from 41% at C_{si} of 0.00068 mole/cm^3 to 83% at C_{si} of 0.0023 mole/cm^3. Further increase in the C_{si} to 0.017 mole/cm^3 resulted into increase in the solute rejection factor to 97.6%. Further increase in the C_{si} became relatively insensitive to solute rejection factor as only marginal increase of 1% was recorded for large increase of C_{si} from 0.017–0.04 mole/cm^3. Hence, three distinct regions of solute rejection factor against C_{si} could be identified. Region #1, spanning C_{si} value range of 0.00068–0.002 mole/cm^3 was the region of rapid rate of increase in solute rejection factor per unit rise in C_{si}. Rate of increase in region #1 was calculated as 5.65% increase in solute rejection factor per unit rise in the solute interfacial concentration.

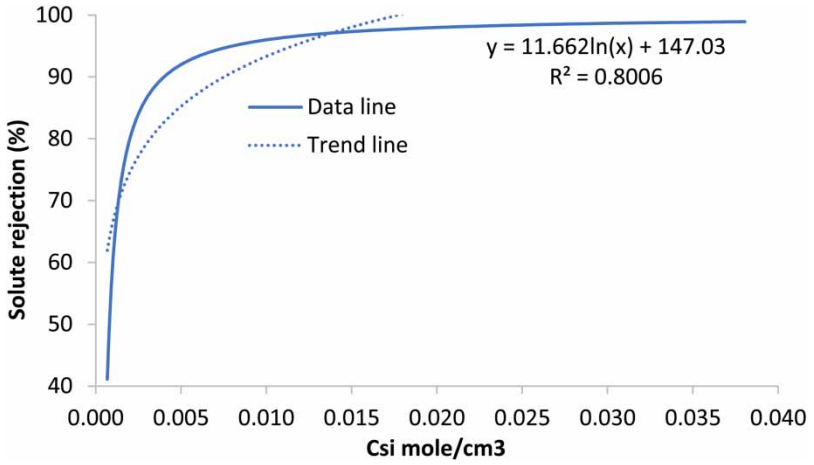

Figure 9 | Solute rejection profile against interfacial solute concentration.

Region #2, spanning C_{si} value range of 0.002–0.017 mole/cm^3 was the region of intermediate rate of increase in solute rejection factor per unit rise in C_{si}. Region #3, spanning C_{si} value range of 0.017–0.04 mole/cm^3 was the region of almost zero rate of increase in solute rejection factor per unit rise in C_{si}. The rate of increase in solute rejection factor per unit rise in C_{si} at regions #2 and #3 were determined as 0.45% and 0.03%, respectively. Region #2 was considered as the optimum operation region having reasonably high solute rejection factor up to 97.6% and intermediate rate of increase in solute rejection factor per unit rise in C_{si}.

3.4. Impact of membrane filter length on specific energy consumption

Figure 10 shows behaviour of the process SEC against variation in the membrane filter length and variation in ΔP. It could be observed that the SEC behaviour had two regions, viz region #1 where the membrane filter length was 1 m and region #2 where the membrane filter length was greater than 1 m. SEC value in region #1 was tending to infinity as its value was 5.3×10^5 kWh/m^3. At region #2 values of SEC were reasonably lower for all values of membrane filter length greater than 2 m. The graph of SEC against ΔP further validated the sectionalization of the SEC behaviour into region #1 having SEC value tending to infinity at higher ΔP greater than 6 atm and region #2 having considerably low SEC value at all values of ΔP.

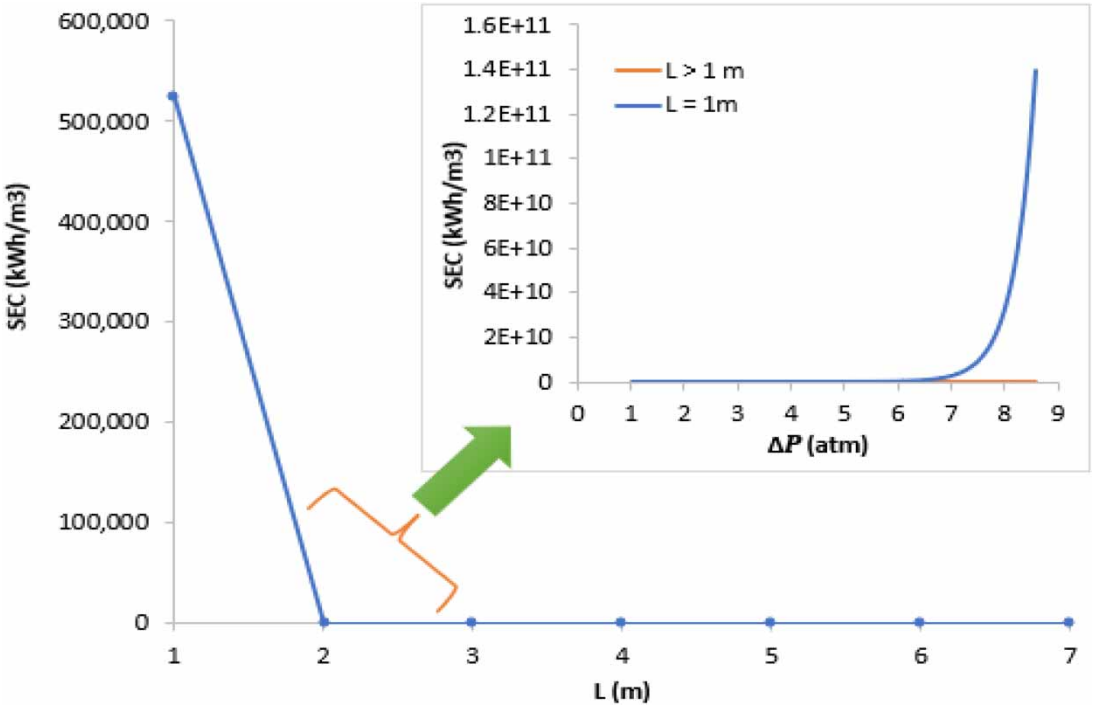

Figure 10 | Specific energy consumption against membrane filter length and ΔP.

Figure 11 shows specific energy consumption profile against membrane filter length at optimum ΔP of 3.7 atm. It could be observed that the SEC requirement of the RO process decreased as the membrane filter length increased. The highest SEC of 317.4 kWh/m^3 was observed at L of 2 m and this dropped by 86% to 43.7 kWh/m^3 when L increased to 3 m. Further increase of L resulted into much more decrease in SEC value. Values of SEC at L values of 4, 5, 6, and 7 m were 14.5, 6.7, 3.7 and 2.2 kWh/m^3, respectively. The SEC value of 3.7 kWh/m^3 obtained at L = 6 m was considered as the optimum SEC as it closely agreed with values reported by other researchers (Tufa *et al.* 2019; Ligaraya *et al.* 2020).

3.5. Impact of RO process parameters on power density and specific energy consumption

Figure 12 shows variation of the power density and specific energy consumption against ΔP at the optimum membrane filter length of 6 m. Both the power density and specific energy consumption increased continuously with rise in ΔP. Both the power density and specific energy consumption had very low and almost similar values at low ΔP less than 3.0 atm. Above ΔP of 3.0 atm, the rate of increase in SEC was clearly higher than the rate of increase in the power density for the same increase in ΔP. The difference became more pronounced as ΔP increased. At the

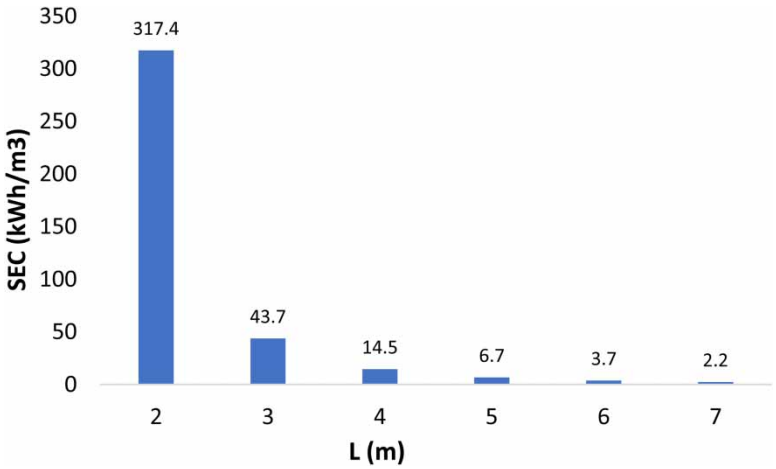

Figure 11 | Specific energy consumption against L at optimum ΔP of 3.7 atm.

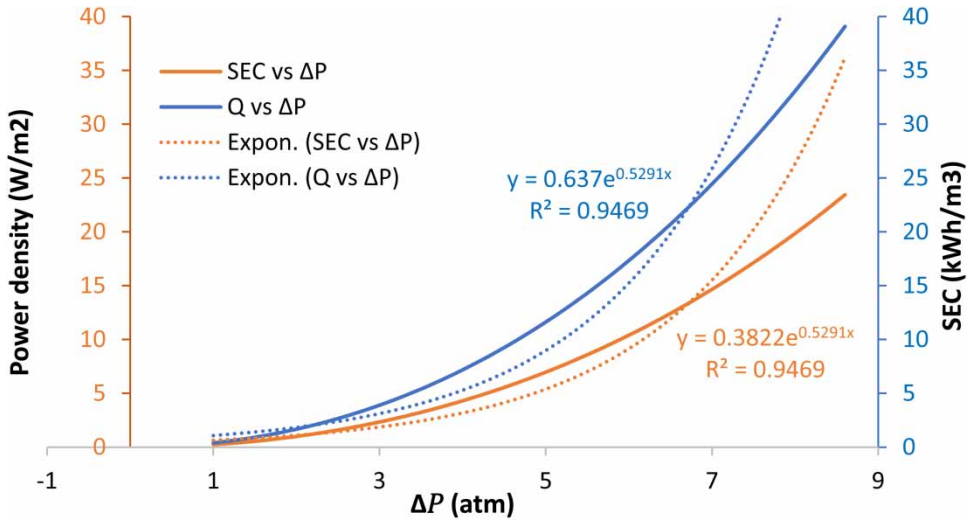

Figure 12 | Power density and specific energy consumption against ΔP.

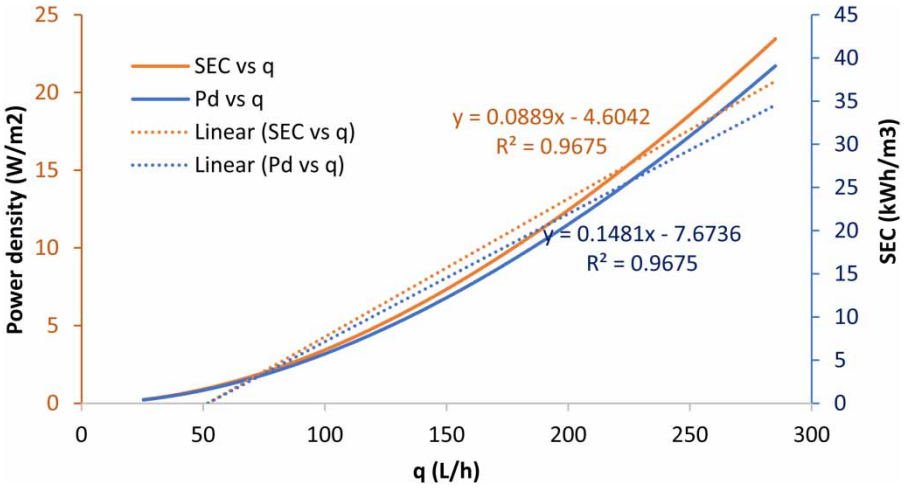

Figure 13 | Power density and SEC against process water output rate.

optimum ΔP of 3.7 atm the specific energy consumption was 3.65 kWh/m^3 and the process power density was 6.09 W/m^2. The optimum SEC and power density values of 3.65 kWh/m^3 and 6.09 W/m^2, respectively, fell within the range of literature energy projection for seawater desalination RO batteries (Tufa *et al.* 2019; Ligaraya *et al.* 2020).

Figure 13 shows the variation of power density and specific energy consumption against process water output rate at the optimum membrane filter length of 6 m. Both the power density and specific energy consumption of the process increased almost linearly with increase in the water output rate. At low water output less than 100 L/h, both the power density and SEC had almost the same values. At higher water output greater than 100 L/h, the rate of increase of SEC per unit increase in water output became higher than the rate of increase of the power density per unit increase in water output. At zero water output rate, the process power density was 4.6 W/m^2 while the specific energy consumption was 7.7 kWh/m^3. Water output of 100 L/h may be considered as the minimum point for a favourable operation of the RO process. At the point of optimum ΔP corresponding to 3.7 atm, the water output rate was 103.2 L/h, and the corresponding power density was 6.09 W/m^2.

4. CONCLUSIONS

Developed model equations have been applied in simulation of the operations of a reverse osmosis process for desalination of seawater at variable ΔP. Simulation carried out at variable ΔP showed that the optimum fluid bulk concentration was $C_o = 0.0004$ mole/cm^3. For simulation carried out at the optimum fluid bulk concentration and a given solute rejection factor, the corresponding values of RO parameters such as the solute interfacial concentration (C_{si}), solute concentration polarity (Γ), water flux (J_w), osmotic pressure ($\Delta\pi$), water output rate (q), power density (Pd) and specific energy consumption (SEC) were determined. It was observed that the RO process operated favourably at $C_o \leq 0.0004$ mole/cm^3, while at $C_o > 0.0004$ mole/cm^3 the process was outrageously in variance with real RO process conditions due to concentration build-up on the bulk side of the membrane. The solute interfacial concentration increased exponentially with increasing values of ΔP. The RO process described by the model operated favourably at $\Delta P < 5.0$ atm. The simulated RO process operated optimally at ΔP of 3.7 atm, C_o of 0.0004 mole/cm^3 and membrane filter length of 6 m. The water flux and average fluid velocity varied linearly with increasing ΔP. Comparison of the water flux against tΔP using literature reports for osmosis direction characterization confirmed that the process proceeded in the reverse osmosis direction. The optimum rate of increase in the solute rejection factor per unit rise in ΔP for the RO process was 0.45% and the optimum solute rejection factor was 97.6%. The power density and specific energy consumption variation with ΔP were both exponential. The optimum water output rate was 103.2 L/h. The optimum specific energy consumption and power density were 3.65 kWh/m^3 and 6.09 W/m^2, respectively. These values compared favourably with literature energy projection for seawater desalination RO batteries.

CONFLICT OF INTEREST STATEMENT

There is no conflict of interest in this work.

DATA AVAILABILITY STATEMENT

All relevant data are included in the paper or its Supplementary Information.

REFERENCES

Amjad, Z. 1993 *Reverse Osmosis: Membrane Technology, Water Chemistry, and Industrial Applications*. Van Nostrand Reinhold, New York, NY.

Cath, T., Childress, A. & Elimelech, M. 2006 Forward osmosis: principles, applications, and recent developments. *Journal of Membrane Science* **281**, 70–87.

Cornelissen, E. R., Harmsen, D. J. H., Blankert, B., Wessels, L. P. & Van der Meer, W. G. J. 2021 Effect of minimal pre-treatment on reverse osmosis using surface water as a source. *Desalination* **1**, 115056.

Henthorne, L. 2009 The current state of desalination. In *IDA World Congress*, Dubai, UAE.

Idrees, M. F. 2020 Performance analysis and treatment technologies of reverse osmosis plant– a case study. *Case Studies in Chemical and Environmental Engineering* **2**, 100007.

Jang, E., Mickols, W., Sujanani, R., Helenic, A., Dilenschneider, T. J., Kamcev, J., Paul, D. R. & Freeman, B. D. 2018 Influence of concentration polarization and thermodynamic nonideality on salt transport in reverse osmosis membranes. *Journal of Membrane Science* **572**, 668–675.

Khawaji, A. D., Kutubkhanah, I. K. & Wie, J. M. 2008 Advances in seawater desalination technologies. *Desalination* **221**, 47–69.

Kim, J., Park, K. & Hong, S. K. 2020 Application of two-stage reverse osmosis system for desalination of high-salinity and high-temperature seawater with improved stability and performance. *Desalination* **492**(114645), 1–14.

Koseoglu, H., Guler, E., Harman, I. B. & Gonulsuz, E. 2018 *Membrane-Based Salinity Gradient Processes for Water Treatment and Power Generation: Chapter 2 – Water Flux and Reverse Salt Flux*. Elsevier B.V, Netherlands, pp. 57–86.

Lee, K. L., Baker, R. W. & Lonsdale, H. K. 1981 Membranes for power generation by pressure-retarded osmosis. *J. Membr. Sci.* **8**, 141–171.

Ligaraya, M., Park, S., Park, J. S., Park, J., Kim, Y. & Cho, K. H. 2020 Energy projection of the seawater battery desalination system using the reverse osmosis system analysis model. *Chemical Engineering Journal* **395**(125082), 1–10.

Lilanea, A., Saifaouia, D., Harissab, D. S., Jenkala, H. & Chouiekha, M. 2020 Modeling and simulation of the performances of the reverse osmosis membrane. *Materials Today Proceedings* **24**(1), 114–118.

Loeb, S. & Sourirajan, S. 1963 Sea water demineralization by means of an osmotic membrane. *Advances in Chemistry* **38**, 117–132.

McCabe, L. W., Smith, C. J. & Harriott, P. 1993 *Unit Operations of Chemical Engineering*, 5th edn. McGraw-Hill, Inc, Singapore.

McCutcheon, J. R. & Elimelech, M. 2006 Influence of concentrative and dilutive internal concentration polarization on flux behavior in forward osmosis. *Journal of Membrane Science* **284**, 237–247.

Monjezi, A. A., Chen, Y., Vepa, R., Kashyout, A. B., Hassan, G., Fath, H. E., Kassem, A. Y. & Shaheed, M. H. 2020 Development of an off-grid solar energy powered reverse osmosis desalination system for continuous production of freshwater with integrated photovoltaic thermal (PVT) cooling. *Desalination* **495**(1), 114679.

Mulder, M. 1997 *Basic Principles of Membrane Technology*. Kluwer Academic Publishers, London. ISBN: 0-7923-4248-8.

Paul, D. R. 2004 Reformulation of the solution-diffusion theory of reverse osmosis. *Journal of Membrane Science* **241**, 371–386.

Salahudeen, N. 2020 Mathematical modeling of reverse osmosis for desalination of seawater. In: *Book of Proceedings of the 3rd International Scientific and Technical Conference, National University of Water and Environmental Engineering*, Petrosani, Romania. pp. 47–49. ISSN 2734–6935.

Scott, K. 1998 *Handbook of Industrial Membranes*. Elsevier Science Publishers Ltd., London, United Kingdom

Tufa, R. A., Gianluca Di Profio, G. D., Fontananova, E., Avci, A. H. & Curcio, E. 2019 Forward osmosis, reverse electrodialysis and membrane distillation: new integration options in pretreatment and post-treatment membrane desalination process. *Membrane Desalination Systems: the Next Generation* **2019**, 365–385.

First received 30 July 2021; accepted in revised form 8 December 2021. Available online 21 December 2021